Developmental Biology 322 (2008) 302–313

Contents lists available at ScienceDirect

Developmental Biology

journal homepage: www.elsevier.com/developmentalbiology

Ionizing radiation-induced gene modulations, cytokine content changes and telomere shortening in mouse fetuses exhibiting forelimb defects

Hanane Derradji [a,*], Sofie Bekaert [b], Tim De Meyer [b], Paul Jacquet [a], Khalil Abou-El-Ardat [a,b], Myriam Ghardi [a], Michaux Arlette [a], Sarah Baatout [a]

[a] Laboratory for Molecular and Cellular Biology Belgian Nuclear Research Centre, SCK·CEN, Boeretang 200, B-2400 Mol, Belgium
[b] Department for Molecular Biotechnology, FBW – Ghent University, Belgium

ARTICLE INFO

Article history:
Received for publication 29 October 2007
Revised 3 July 2008
Accepted 25 July 2008
Available online 7 August 2008

Keywords:
Limb defect
Radiation
Teratogenesis
Apoptosis
Telomere shortening
Inflammation
Cytokines
Signal transduction

ABSTRACT

Several lines of evidence have linked limb teratogenesis to radiation-induced apoptosis and to the p53 status in murine fetuses. In previous reports, we studied the occurrence of various malformations after intrauterine irradiation and showed that these malformations were modulated by p53-deficiency as well as by the developmental stage at which embryos were irradiated. In this new study, we focused onto one particular phenotype namely forelimb defects to further unravel the cellular and molecular mechanisms underlying this malformation.

We measured various parameters expected to be directly or indirectly influenced by irradiation damage. The mouse fetuses were irradiated at day 12 *p.c.* (*post conception*) and examined for forelimb defects on gestational days 15, 16, 17 and 19 of development. The release of inflammatory cytokines was determined in the amniotic fluid on day 16 *p.c.* and the mean telomere lengths assessed at days 12, 13 and 19 *p.c.* Differential gene expression within the forelimb bud tissues was determined using Real Time quantitative PCR (RTqPCR) 24 h following irradiation. Apoptosis was investigated in the normal and malformed fetuses using the TUNEL assay and RTqPCR.

First, we found that irradiated fetuses with forelimb defects displayed excessive apoptosis in the predigital regions. Besides, overexpression of the pro-apoptotic Bax gene indicates a mitochondrial-mediated cell death. Secondly, our results showed overexpression of MKK3 and MKK7 (members of the stress-activated MAP kinase family) within the malformed fetuses. The latter could be involved in radiation-induced apoptosis through activation of the p38 and JNK pathways. Thirdly, we found that irradiated fetuses exhibiting forelimb defects showed a marked telomere shortening. Interestingly, telomere shortening was observed as the malformations became apparent. Fourthly, we measured cytokine levels in the amniotic fluid and detected a considerable inflammatory reaction among the irradiated fetuses as evidenced by the increase in pro-inflammatory cytokine levels.

Altogether, our data suggest that transcriptional modulations of apoptotic, inflammation, stress, and DNA damage players are early events in radiation-induced forelimb defects. These changes resulted in harsh developmental conditions as indicated by a marked increase in cytokine levels in the amniotic fluid and telomere shortening, two features concomitant with the onset of the forelimb defect phenotype in our study.

Introduction

Vertebrate limbs have provided an excellent model system to investigate morphogenesis and the mechanisms behind limb teratogenesis. In this context, a number of studies reported the teratological properties of various chemicals (thalidomide, warfarin, valproic acid, and retinoic acid), hyperthermia, alcohol, drugs (cocaine) and irradiation (Wang et al., 1999; Tiboni et al., 1998, Layton and Hallesy, 1965).

The embryopathic action of the various teratogens is type-specific. While thalidomide affects the insulin-growth factor 1 and fibroblast growth factor 2 pathways during development, irradiation would act via apoptosis to induce limb defects. Earlier studies showed that radiation-induced limb defects were closely linked to the p53 (the so-called guardian of the genome) status and to the dose of irradiation. For the same dose of radiation, digital defects were high in the wild type (p53+/+), intermediate in the heterozygous (p53+/−) and low in the knock out mice (p53−/−). This suggests a causal role for p53-dependent apoptosis in the development of malformations (Boreham et al., 2002; Wang, 2001; Wang et al., 2000, 1999). However, other studies believe in the protective effect of the p53 against radiation-induced teratogenesis as p53 would eliminate the damaged cells via

* Corresponding author. Fax: +32 14 31 47 93.
E-mail address: hderradj@sckcen.be (H. Derradji).

0012-1606/$ – see front matter © 2008 Elsevier Inc. All rights reserved.
doi:10.1016/j.ydbio.2008.07.032

apoptosis (Norimura et al., 1996). These paradoxical effects have been related to the difference in the time of irradiation (early or late organogenesis).

Besides apoptosis, irradiation triggers other responses such as inflammation, stress-activated kinases and telomere shortening (Bekaert et al., 2005, Zhou et al., 2003, Dent et al., 2003). However, no study reported their involvement or association in a forelimb defect phenotype. In the present work, we investigated these responses to assess whether they are associated with forelimb defects in p53+/+ mouse fetuses, X-irradiated in late organogenesis stage (day 12 *p.c.*).

The first part of this work was dedicated to a morphological study, to describe the forelimb defects induced upon X-irradiation of the fetuses. Using a stereomicroscope, mouse fetuses were examined for the presence of forelimb defects at gestational days 14, 15, 16, 17 and 19. The choice of giving the mouse fetuses 3 Gy of X-irradiation at day 12 *p.c.* relied on a previously described model of limb defects (Wang, 2001). Indeed, using these parameters, we ensured the occurrence of 100% of forelimb defects, a prerequisite condition for the next parts of the work, where no possible distinction between normal and abnormal forelimbs could be made by a simple observation under a stereomicroscope.

The second part of this work was a molecular and cellular oriented-study. We investigated gene expression modulations 24 h following irradiation (day 13) in normal and abnormal fetuses. For that, we examined the expression of genes related to the Mitogen Activated Protein kinase superfamily (MAPK) (MKK3 and MKK7), apoptosis (Bax, Bcl-2 and caspase-3) and DNA damage response (ATM, RAD17 and 53BP1) as they are all part of the response following an irradiation insult.

We previously reported that irradiation of the mouse gastrula (day 8 *p.c.*) with 0.5 Gy of X-rays with different p53 status, resulted in an increased frequency of congenital malformations (exencephaly, gastroschisis, cleft palate, polydactyly, dwarfism) among the fetuses with impaired p53 genotype (+/− and −/−) (Baatout et al., 2002). The latter, were shown to have abnormal telomere shortening as assessed within fetal soft tissue samples (Bekaert et al., 2005). In an attempt to explore the timing of telomere damage during development we measured telomere lengths in normal and irradiated fetuses exhibiting the particular forelimb defects.

Cytokines, as well as chemokines, represent important mediators of the inflammatory reaction and several studies revealed an increased serum level of pro-inflammatory cytokines in response to a number of inducing stimuli and pathogenesis (i.e. microbes, toxins, oxidative stress, aging and bowel diseases) (Sarkar and Fisher, 2006; Bamias et al., 2005; Farber et al., 1990). In addition, knowing that oxidative stress and inflammation are potential accelerators of telomere shortening, we measured the pro-inflammatory cytokine/chemokine levels in the amniotic fluid of the fetuses to check whether inflammation was linked to forelimb defects.

In this work we shed light on the various cellular and molecular events down- and upstream of apoptosis, that could be associated with forelimb defects following irradiation of mouse fetuses during late organogenesis.

Materials and methods

Experimental animals

C57BL/6J mice were maintained in a conventional animal facility in accordance with the institutional guidance for the care and use of laboratory animals. They were obtained from Janvier Laboratories (Le Genest-Saint-Isle, France) and were housed in plastic cages under controlled temperature (23±2 °C) and relative humidity (55±10%) with a 12 h light/12 h dark cycle. Pellet food and tap water were freely available.

Females were mated with males during 2 h (from 5 a.m. to 7 a.m.). Gestational day 0 for each mouse designated the day of the vaginal plug. The animals were kept in the conventional animal facility until use.

Irradiation

Irradiation of the mice with 3 Gy was performed at day 12 *p.c.* with a Pantak HF420 RX machine operating at 250 kV, 15 mA, 1 mm Cu filtration and at a dose rate of 0.375 Gy/min. Dosimetry was performed on a regular basis with a 0.6 cm^3 ionization chamber (NE 2571), which was connected to a dosemeter (Farmer dosemeter 2570). The chamber was placed in parallel to the irradiated mice. Dose heterogeneity was evaluated as being <1.5%. Control mice were not irradiated but otherwise treated like the irradiated ones (sham mice).

Fetus collection and skeletal staining

For the teratological and skeletal studies, 12 dams in the irradiated group and 8 dams in the control group were sacrificed by cervical dislocation on day 19 *p.c.*

Uteri were excised and the number of live and dead fetuses was scored. Fetuses were then screened for forelimb abnormalities under a stereomicroscope before being subjected to a double staining of cartilage and bone (Kimmel and Trammell, 1981). Briefly, after complete skinning and evisceration of the fetuses, staining was performed overnight using a mixture of 0.14% alcian blue (for cartilage) and 0.12% alizarine red (for bone) in a mixture of ethanol and glacial acetic acid (50v/8v). The specimens were next digested with 2% KOH, then cleared and hardened in a 1:1 mixture of distilled water and glycerin. Long-term storage of the specimens was performed in pure glycerin at room temperature.

Measurement of the forelimb bone length and classification of the digit abnormalities

After having examined and classified the skeletal preparations into the different forelimb defect categories as described in Kurishita (1989), the length of the stylopod (the most proximal element of a limb that will give rise to humerus in the forelimb), zeugopod (the intermediate elements of a limb that will give rise to radius and ulna in the forelimb) and autopod (distal elements of a limb that will give rise to the wrist and fingers in the forelimb) segments issued from control and irradiated groups were measured using the ImageProPlus 4.5 imaging software (Media Cybernetics, Silver Spring, MD).

In situ apoptosis detection

Fetuses were fixed with 4% PFA/PBS overnight at 4 °C and then processed for a series of dehydratation/paraffinisation (Gavrieli et al., 1992) using an enclosed tissue processor instrument (PathcentreTM, Shandon). Paraffin blocks containing the forelimb buds were cut in 8-µm thick sections. The sections were put on poly-L-lysine treated slides and apoptotic cells were detected using the TUNEL assay based on fluorescein-dNTP incorporation (In situ Cell Death Kit, Roche, Germany). Briefly, the sections were deparaffined and rehydrated then treated with the TUNEL reaction mixture (containing the terminal deoxynucleotidyl transferase (TdT) enzyme). Apoptotic cells appeared in green when viewed under a fluorescence microscope.

RNA extraction

Total RNA was extracted at day 13 *p.c.* from forelimb bud tissues of either control or irradiated fetuses. Under a stereomicroscope, forelimb buds were dissected in ice cold PBS supplemented with 0.1% DEPC (Diethyl pyrocarbonate) (Sigma-Aldrich, Steinheim,

Table 1
Number of digits observed in the irradiated mouse fetuses

Number of digits	Percentage
1	23.3
2	8.5
3	43
4	18.5
Stump (undistinguished number of digits)	5.7

Germany), then immediately snap frozen in liquid nitrogen. Total RNA was isolated from 8 forelimb buds in each group using the TRIZOL RNA isolation reagent (Sigma-Aldrich) followed by a DNase I treatment. The isolated total RNA was assessed for its quality and concentration using a 2100 Bioanalyzer (Agilent Technology, Waldbronn, Germany). RNA was then stored at −80 °C until used.

Real time quantitative PCR

Real Time quantitative PCR (RTqPCR) was used in order to investigate changes in gene expression between the control and the irradiated groups. Template total RNA (2 μg) was reverse transcribed using the TaqMan reverse transcription kit (Applied Biosystem) with oligo(dT) under the following thermal cycle: 25 °C/2 min, 48 °C/30 min and 95 °C/5 min. It was then chilled on ice. The aliquots of generated cDNA were amplified using a house designed pair of primers (Primer express 2.0 software, Applied Biosystems, Foster, CA) corresponding to the gene of interest. Quantitative Real Time PCR was carried out in an ABI Prism 7500 sequence detector (Applied Biosystems) using Syber Green reagent (qPCR mastermix plus for Syber Green I, Applied Biosystems). The PCR cycle parameters were: 50 °C/2 min, 95 °C/10 min, followed by 45 cycles of denaturation at 95 °C/15 s and primer extension at 60 °C for 1 min. The specificity of the PCR products was confirmed by examination of products melting curves. Changes in relative gene expression between cDNA samples were determined using ΔΔCt method in which the Rpl13 (Ribosomal protein l13) gene was used for normalization since it appeared to be the most stable amongst the house keeping genes (Act-b, HPRT-1, TRFC, Gyk, 18 s, GAPDH, Tpb and Ubc) tested in our system.

Telomere Restriction Fragment (TRF) analysis

Genomic DNA was extracted from the flank regions of the frozen fetuses using a DNA Purification kit (PuregeneTM, Gentra Systems, Minneapolis). 5 μg of the genomic DNA were used to assess mean telomere length using TRF analysis as previously described (Bekaert et al., 2005). Although the image was digitally enhanced, blot analysis and calculation of mean TRF values were performed on the raw images (in Matlab 7.0, Mathworks, Natick, Massachusetts, USA). Simple weight points were calculated for every lane based on the intensities between 5 kb and 150 kb and subsequently transformed into molecular weights (mean TRF values) using loglinear regression based on the marker fragments as previously described (Bekaert et al., 2005).

Cytokine measurement in the amniotic fluid using multiplex bead array

Amniotic fluid was collected at day 16 of development where it reaches its highest level (Renfree et al., 1975). Uteri were removed and amniotic fluid was harvested by insertion of a fine pipette directly into the amniotic cavity, carefully avoiding puncture of the yolk sac or allantoic vessels. Directly after collection, amniotic fluids were centrifuged (8 min at 7000 rpm) and the supernatant treated with aprotinin to a concentration of 500 KIU/ml to prevent cytokine degradation (Porter et al., 2001). For long-term storage, amniotic fluid samples were stored at −80 °C.

39 cytokines were measured in total in single 50 μl aliquots of amniotic fluids from control and irradiated fetuses using the multiplex bead array assay (Luminex). Microspheres were dyed with different concentrations of two fluorophores to generate distinct bead sets. Briefly, each bead set was coated with capture antibodies specific for one particular cytokine (i.e. IL-6, IFN-gamma). Captured cytokines present in the amniotic fluid were detected using a biotinylated detection antibody tagged with streptavidin-phycoerythrin (S-PE). The Luminex 100 analyzer (or multiplex array assay analyser) which is a dual laser, flow-based, sorting and detection platform was used for quantifying 39 cytokines concomitantly in each amniotic fluid sample (Rules Based Medicine, Austin, Tx, USA). This machine is equipped with one laser which is bead-specific and determines which cytokine is being detected whilst the other laser determines the magnitude of PE-derived signal, which is in direct proportion to the concentration of cytokine present in the sample.

Statistical analysis

The results were analyzed using SPSS 12.0. The differences of the various end-points between control and irradiated groups (bones length, amniotic fluid content, gene expression and TRF analysis) were analyzed using the one way ANOVA followed by a Tukey's *post hoc* comparisons, preceded by confirmation of the equality of variances and normality of the distributions by Levene's and Kolmogorov–Smirnov tests, respectively. Results were considered as significantly or highly significantly different from each other when the probability values were $p \leq 0.05$ and $p \leq 0.01$, respectively.

Results

Presence of forelimb defects in all irradiated fetuses

To assess the frequency of fetuses displaying forelimb defects upon irradiation, we performed a teratological study of the forelimbs on 105 fetuses issued from 12 irradiated dams (average of 8.75 fetuses/dam). Under a stereomicroscope, each fetus was carefully examined for viability and forelimb defects. Body weight was also measured.

In the irradiated group, 26.6% of the fetuses were dead at the time of dissection, while no dead fetus was scored in the control group. Besides, fetuses issued from the irradiated group had reduced body weight in comparison to the control group (0.47 g±0.07 versus 1.09 g±0.12, respectively). A fetus was classified as a dwarf if it weighted less than 75% of the mean of the group (Jacquet et al., 1995).

Regarding forelimb defects, 210 forelimbs (right and left) from the irradiated fetuses were checked for the number of digits and dorso-ventral identities. All of them showed hypodactyly (reduction in the number of digits) but no defect in the dorso-ventral identity was noticed. In contrast, all control fetuses showed a normal forelimb profile with 5 distinct digits at both limbs.

When counting the number of digits in all fetuses, 43% of the examined fetuses had 3 digits, 23% exhibited one digit and 18.5% had 4

Table 2
Digit configurations observed in forelimbs issued from irradiated mouse fetuses

Phenotype code	Number of digits	Percentage
A	3+3	35, 2
B	1+1	17, 1
C	4+4	15, 2
D	2+2	6, 6
E	Stump	5, 7
F	3+1	11
G	4+3	4, 5
H	1+2	1, 9
I	4+2	1, 9
J	3+2	0, 86

The numbers of digits are reported as: left forelimb+right forelimb.

digits (Table 1). When considering only the fetuses with the same number of digits in each forelimb, 10 distinct phenotypes were observed among the irradiated group (Table 2): 35.2% exhibited 3 digits (phenotype "A"), 17% had 1 digit (phenotype "B"), 15% showed 4 digits (phenotype "C") and 6.6% had 2 digits (phenotype "D") (Fig. 1). The remaining samples (corresponding to 25.86%) had different phenotypes on both autopods (Table 2).

Radiation-induced external forelimb defects are associated with skeletal alterations of bony elements

Skeletal preparations from 53 randomly selected irradiated fetuses (19 days *p.c.*) were used to examine and to measure the bony elements constituting the forelimbs. Description of the digital defects was made following the glossary previously established by Kurishita (1989). The majority of forelimb defects consisted of osseous or cutaneous syndactyly (fusion of adjacent fingers or osseous elements) (99 and 71%, respectively), ectrodactyly (metacarpal and phalanxes missing) (80%) and aphlangy (metacarpal present but phalanxes missing) (49%). Pictures of the whole-mount skeletons of forelimbs bearing different types of digital malformations are shown in Fig. 2 and the percentages of the various forelimb malformations are represented in Fig. 3. In nearly all the cases (98%), coexistence of these malformations within a given forelimb was observed.

Each digit was involved in a specific proportion to the various forelimb defects observed. Indeed, osseous syndactyly concerned in the majority (77%) digits 4 and 5, while the cutaneous syndactyly involved digits 4 and 3 (39.62%). Ectrodactyly concerned digit 2

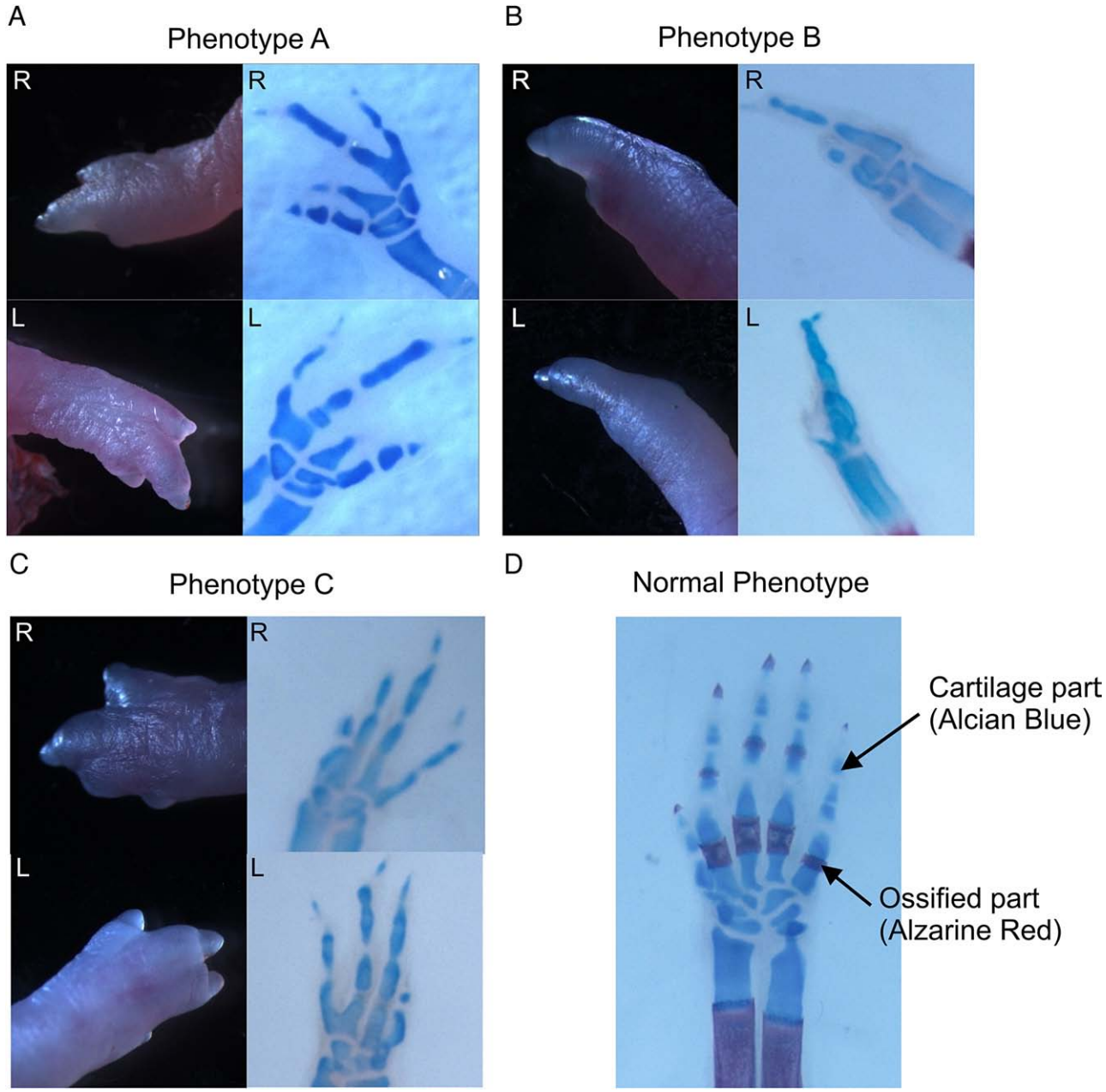

Fig. 1. Major abnormal forelimb phenotypes observed in the irradiated mouse fetuses at day 19 *p.c.* In panels A–D, the photos on the left are stereomicroscope images of the forelimbs of fetuses while the photos on the right are skeletal preparations done by KOH digestion and double staining with alizarine red and alcian blue (R: Right; L: Left). (A) Images representing forelimbs with only three distinguishable digits; (B) images representing forelimbs with a single distinguishable digit; (C) images representing forelimbs with four distinguishable digits; (D) a skeletal preparation of a normal forelimb with all five digits intact and with the cartilage part stained with alcian blue and the ossified part stained with alizarine red. All photos were taken at day 19 *p.c.*

in 64.5% of the cases and aphlangy concerned exclusively digit 3 (Fig. 2).

Deficiency in the ossification was obvious in all skeletal preparations issued from irradiated fetuses as indicated by the negative alizarine red staining in the regions (like in the mid-metacarpals and phalanxes) normally ossified at the time of fetal development. Bony elements constituting the forelimb were present but severely reduced in size in all irradiated mouse fetuses (Fig. 4). Stylopod was present but sometimes thinner than normal. In a few cases the humerus element appeared fused to the scapula. Zeugopod contained often bended but always present ulna and radius; except in one case, where a single radius element was present. Autopod showed many missing and fused carpals (Fig. 5). We then monitored the presence of forelimb defects at different time points during fetal development. Surprisingly, hypodactyly only became phenotypically apparent at day 19 *p.c.* On the contrary, fetuses at days 14, 15, 16 and 17 *p.c.* showed 5 distinguishable digits at both forelimbs (Fig. 6). These data suggest that apoptosis might be involved in limb reduction defects.

Radiation-induced increase of apoptosis is associated with malformation

In order to study apoptosis, TUNEL assay was performed on forelimb bud sections at days 13 and 16 *p.c.* Observation of the tissue sections under a fluorescent microscope revealed that apoptosis was clearly enhanced in irradiated fetuses (Figs. 7B and D). In the control sections, the majority of apoptotic cells were located all over the margins of the autopods (Fig. 7A) and in the interdigital tissue (Fig. 7C). In contrast, in the irradiated fetuses, the apoptotic cells were spread in the malformed autopods (including the predigital and interdigital regions) (Figs. 7B and D).

Radiation-induced increased of cytokine and chemokine concentrations in the amniotic fluid Cytokines and chemokines are multifunctional mediators of biological responses to tissue damage. Alteration in their profile may either block (IL-1 and CSF) or enhance apoptosis (TNF-α). In addition, there are compelling evidences for the

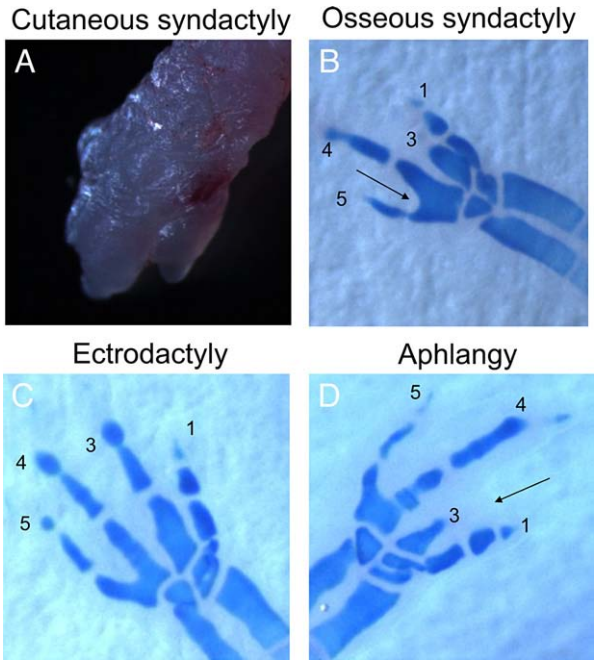

Fig. 2. Radiation-induced cutaneous and skeletal defects observed in the autopodium segment at day 19 *p.c.* Syndactyly, the fusion of two adjacent elements, at the cutaneous level (A) or osseous level (B) (seen here at, arrow). Ectrodactyly, the disappearance of whole digits due to osseous element loss (C; loss of second digit). Aphlangy, the loss of part of a digit (D; loss of the third phalanx but not the metacarpal; arrow).

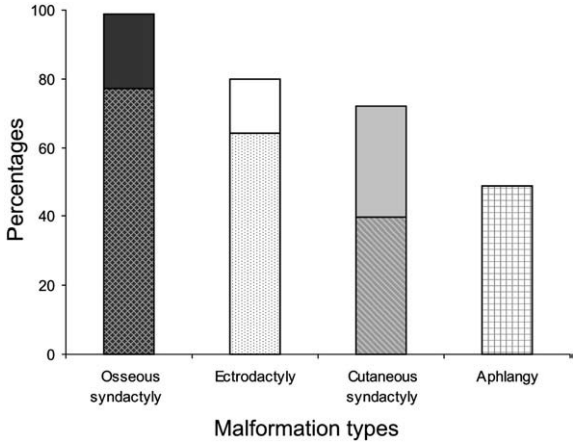

Fig. 3. Major autopod defects observed at day 19 *p.c.* in irradiated fetuses. Osseous syndactyly was the most observed and constituted 99% of cases of which 77% involved metacarpals 4 and 5 (non-solid part). Ectrodactyly was observed in 80% of the cases of which 64.5% appeared in the second digit (dotted). Cutaneous syndactyly appeared in 71% of fetuses of which 39% involved digits 3 and 4 (striped). Finally, aphlangy was the least observed and it appeared in 49% of the fetuses where digit 3 was exclusively concerned. Overlap of these phenomena was not uncommon in the irradiated fetuses.

detrimental effects of pro-inflammatory cytokines/chemokines on pregnancy outcome. Indeed, high levels of IL-6, IL-10, MCP-1, IL-8,TNF-α and IFN-γ in the amniotic fluid have been associated with low birth weight, preterm labor, hyperechogenic bowel disorder and chorioamnionitis (Orsi et al., 2007; Esplin et al., 2005; Orsi et al., 2006; Oboh et al., 2006; Goepfert et al., 2004; Bartha et al., 2003). In this study, the pro-inflammatory profile was explored in the amniotic fluid to identify physiological markers of limb defect phenotypes observed following irradiation.

Using the multiplex array assay, a total of 39 cytokines and chemokines were detected in 50 μl of amniotic fluid from 5 irradiated and 5 control samples. The results of cytokine and chemokine concentrations in the two groups are summarized in Table 3. Cytokine concentrations were in the majority highly increased in the irradiated group in comparison with the control ones. However, a few cytokines showed an opposite profile (6 cytokines). Other cytokines were undetectable suggesting either their absence in our samples or their presence in quantities below the detection limit of the methodology.

Radiation-induced shortening of telomeres at day 19 p.c.

Although telomere biology plays an important role in transducing the apoptotic signals and was previously shown to be involved in congenital defects (Bekaert et al., 2005), there is still a considerable lack of information regarding telomere dynamics during development. Since telomere length has been associated with inflammatory

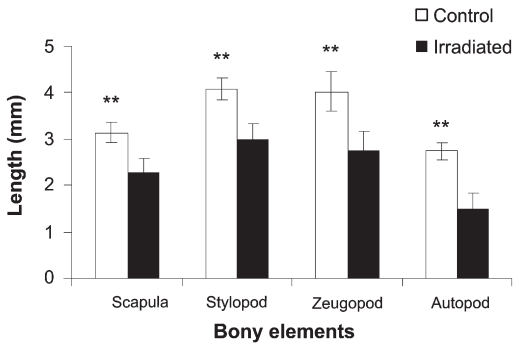

Fig. 4. Comparison at day 19 *p.c.* of the length of the bony elements constituting the forelimb in the control and irradiated fetuses. The bones of the forelimbs of irradiated fetuses were consistently shorter than those of their normal counterparts $^{**}p<0.01$.

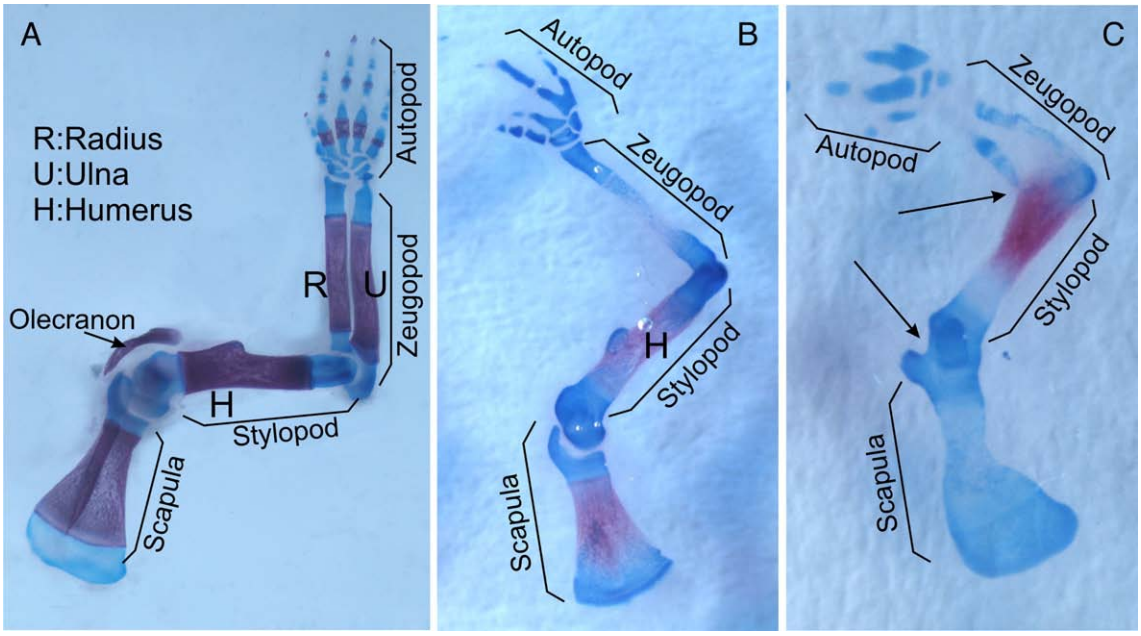

Fig. 5. Radiation-induced changes in the forelimb skeletal elements. Skeleton of normal (A) and irradiated (B, C) fetuses. The bones of irradiated fetuses showed bending and misossification (B and C) as well as fusion of zeugopod to stylopod (B) and fusion of stylopod to both scapula and zeugopod (C, arrows). Missing digits and fused or missing carpals and metacarpals were observed in the autopodium. The olecranon was completely absent (C, lower arrow) as well as the ulna in one case (B).

markers, such as the cytokine IL-6 (Bekaert et al., 2007), we evaluated whether the increased inflammation and apoptosis might also be featured by accelerated telomere attrition in damaged tissue of specific malformed phenotypes of forelimb defects.

TRF analysis was used to measure telomere length in irradiated and control fetuses at different developmental time points following irradiation (6 h, 24 h and 7 days, respectively). Fig. 8A shows smears corresponding to telomere signals from each condition under examination.

Results of telomere length estimation are depicted in Fig. 8B. In fetuses at day 19 *p.c.*, TRF means were significantly different in irradiated and control fetuses ($p<10^{-12}$), Interestingly, when considered separately, irradiated and control day 19 fetuses had significantly lower mean TRF values than all the other groups (days 12 and 13, each time $p<0.00001$). For the groups of fetuses at days 12 and 13 *p.c.*, no significant difference in the mean TRF values were observed between the irradiated and control fetuses ($p>0.3$ for each separate test). Although the results suggest lower mean TRF values at day 13 *p.c.* compared to day 12 *p.c.* these differences were not significant.

Radiation-induced differences in gene expression profiles

To investigate whether transcriptional modulations of key players in apoptosis (Bcl-2, Bax and caspase-3) and inflammation (IL-6, IL-4, MCP-1, IP-10 and CD4) might underlie such events, we checked their expression profile among control and irradiated fetuses. In addition,

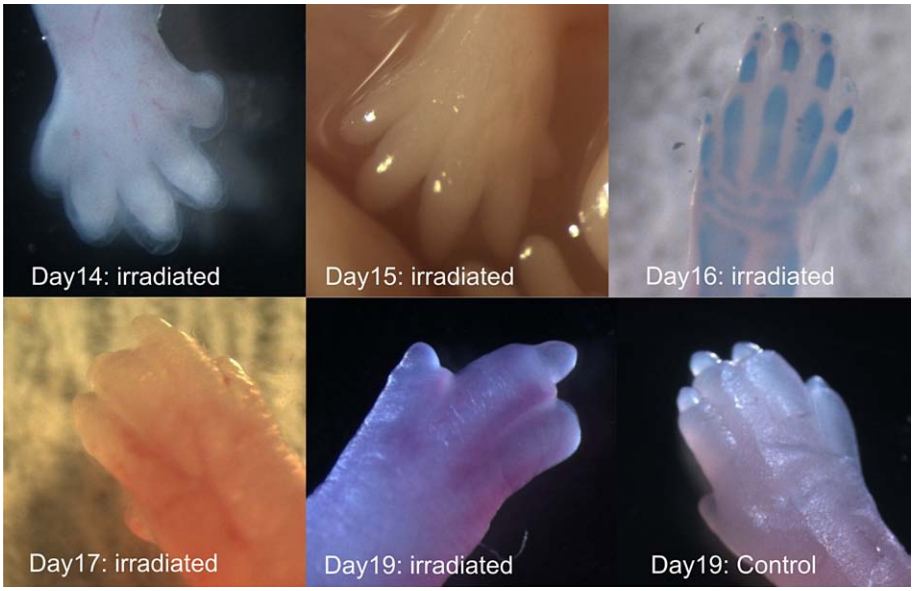

Fig. 6. Survey of radiation-induced forelimb defects. Days 14 and 15 *p.c.* irradiated fetuses with normal forelimbs (five digits) (first two photos). The forelimbs of irradiated fetuses at 16 and 17 days *p.c.* with misossified and crooked bones but with full number of digits (third and fourth pictures). Absence of digits in the forelimb of irradiated fetus at 19 days *p.c.* (fifth picture). Normal forelimb with all digits intact of control fetus at 19 days *p.c.* (last picture).

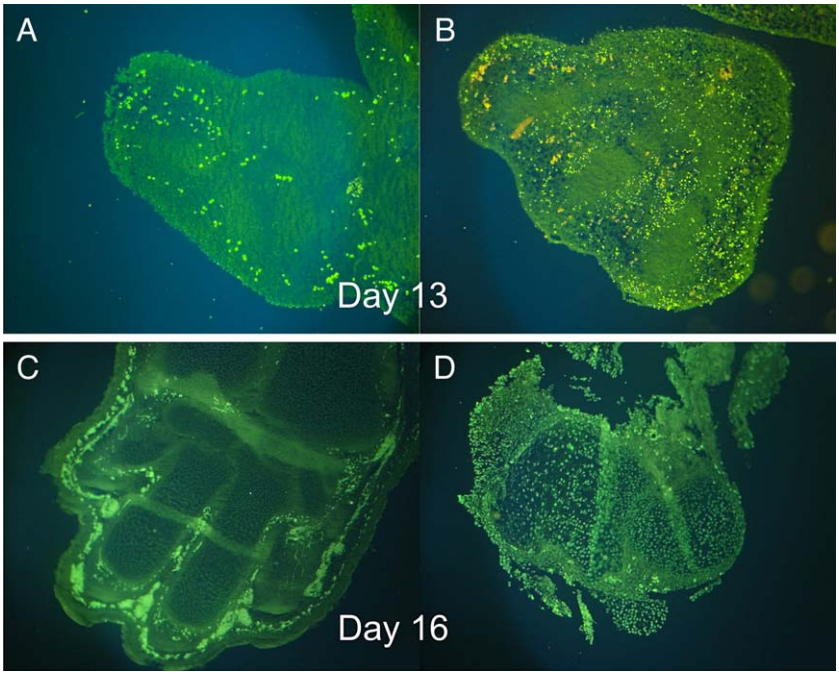

Fig. 7. TUNEL assay on forelimb sections. Whole mount images of control (A, C) and irradiated (B, D) forelimbs of 13 and 16 days *p.c.* fetuses, respectively. Brightly stained spots are apoptotic cells which are confined to discrete regions in normal forelimbs (A, C) where apoptosis is necessary for development (separation of digits) while they are more widespread in irradiated forelimbs (i.e. interdigital space) (B, D).

knowing that irradiation is a stimulator of the stress and DNA damage responses, we screened the expression of important regulators of the MAP kinase pathway (MKK3 and MKK7) and DNA damage response (Ataxia Telangectasia Mutated ATM, Rad17 and 53BP1). More importantly, ATM, Rad17 and 53BP1 were shown to be associated with critically short telomeres (Takai et al., 2003). The results are displayed in Fig. 9.

In the irradiated conditions, we observed a higher expression of MKK3, Rad17, ATM, 53BP1 and MKK7 genes (Figs. 9A and B). Expression of Bax was markedly higher compared to caspase-3 and Bcl-2 expressions (Figs. 9C and D) suggesting an imbalance between the pro-apoptotic (Bax and caspase-3) and the anti-apoptotic mediators that resulted in a rapid onset of cellular death as observed by a positive TUNEL assay at day 13 *p.c.* in irradiated fetuses. Furthermore, in contrast to IL-4 and 6, gene expression profiles of CD40, MCP-1 and IP-10 cytokines were increased in the irradiated group (Figs. 9E and F).

Discussion

Radiation-induced forelimb defects in the fetuses during late organogenesis

In the present work, we examined the external abnormalities caused by irradiation of mouse embryos during late organogenesis (day 12 *p.c.*). The only gross malformations observed were forelimb reduction defects combined with dwarfism and general oedema. This is obviously related to the developmental stage at which the radiation exposure occurred. Irradiation would have induced a large panel of malformations, eventually leading to embryonic death, if exposure had taken place during the early organogenesis period. Previous studies performed in our laboratory and elsewhere have shown that such effects are dependent on the p53 status of the embryos (Wang, 2001; Baatout et al., 2002). In the present study, irradiation occurred at a time when the organs are so well formed that malformations could hardly be induced, except those of distal organs such as limbs (Wang, 2001).

Excessive cell death may underlie radiation-induced limb teratogenesis

In our study, apoptosis was detected 24 h after irradiation by both TUNEL assay and gene expression analysis (RTqPCR). Bax is a pro-apoptotic factor that triggers the release of pro-apoptotic mediators such as cytochrome c and causes mitochondrial dysfunction, which in turn activates the initiator caspase 9 and thereafter caspase 3. Expression of Bax in the irradiated samples was significantly higher than in the controls (Fig. 9D). Expression of the pro- and anti-apoptotic members, caspase-3 and Bcl-2, respectively, was also higher in the irradiated group. Although Bcl-2 was present at the transcriptional level, it failed to antagonize the apoptotic effects of Bax. This might be due to an insufficient Bcl-2 expression or to an unsuccessful change in Bcl-2 conformation necessary for Bax inhibition (Dlugosz et al., 2006). A possible consequence of the high imbalance between the pro- and anti-apoptotic factors is mitochondrial dysfunction and the release of cytochrome c and AIF (apoptosis inducing factor, a final effector of mitochondrial apoptosis) that will both ultimately induce cell death.

Interestingly, apoptosis was still observed in the forelimb tissues several days after irradiation (day 16 *p.c.*), as shown by the TUNEL assay (Figs. 7B and D). This could result from the development of a chromosomal instability in the progeny of irradiated cells and/or from the inflammatory reaction occurring in the tissues surrounding the fetuses. Indeed, earlier studies showed that irradiation of one-cell mouse embryos led to an increase of structural and numerical chromosomal aberrations in the three subsequent mitotic divisions (Pampfer and Streffer, 1989; Weissenborn and Streffer, 1988). Moreover, chromosomal aberrations were still observed in mouse fibroblasts 19 days following the irradiation of the embryo at the one-cell stage. After a dose of 2 Gy, the yield of chromatid fragments in the fibroblasts reached as much as 27.5%. Such aberrations are clearly not compatible with cell survival (Pampfer and Streffer, 1989). In our case, we assume that irradiation of the fetuses with 3 Gy at day 12 *p.c.* affected the genomic DNA in such a way that new chromosomal breaks incompatible with cell survival developed in much later cell generations (day 16 *p.c.*) without any further exposition (Streffer, 2006). In

Table 3
Comparison between cytokine and chemokine concentrations measured in the amniotic fluid of control and irradiated fetuses using the multiplex bead array assay technology (*$p<0.05$; **$p<0.01$)

Cytokines and chemokines (pg/ml)	Cytokine and chemokine names	Cytokine and chemokine Concentrations (pg/ml)		
		Controls (mean±SD)	Irradiated (mean±SD)	Ratio (control/irradiated)
CD40	CD40**	123.5±16.82	228.25±14.86	0.54
Haptoglobin	Haptoglobin**	850±150	1630±330	0.52
IFN-γ	Interferon-gamma**	9.6±0.65	16.45±1.33	0.58
IP-10	Inducible protein-10**	62.45±11.89	499.59±211.22	0.13
RANTES	Regulation upon activation, normal T-cell expressed and secreted*	4110±190	6880±1840	0.60
OSM	Oncostatin M**	80.0±10	110±9	0.73
SCF	Stem cell factor**	184.70±17.55	383.25±34.56	0.48
MCP-3	Monocyte chemoattractant protein-3**	1675.0±311	5517.50±895.7	0.30
MCP-1	Monocyte chemoattractant protein-1**	1545.0±524.11	7312. 50±356	0.21
MIP-1beta	Macrophage inflammatory protein-1beta	127±6.16	460.75±152.09	0.28
MIP-1gamma	Macrophage inflammatory protein-1gamma**	4800±910	7640±1360	0.61
MIP-2	Macrophage inflammatory protein-2*	17.97±3.93	30.65±7.53	0.59
IL-4	Interleukin-4*	11.65±0.98	15.3±1.19	0.76
IL-6	Interleukin-6*	12±2.82	17.7±2.44	0.68
IL-7	Interleukin-7**	30±8	46±4	0.65
IL-10	Interleukin-10**	299.25±9.50	412.25±33.59	0.73
IL-11	Interleukin-11*	11930±2120	14640±850	0.81
IL-12p70	Interleukin-12p70**	90±9	143±42	0.63
IL-17	Interleukin-17*	11±1	17±5	0.65
TNF-alpha	Tumor necrosis factor-alpha**	57±10	83±5	0.69
Lymphotactin	Lymphotactin**	24.37±5.27	34.55±1.4	0.71
VEGF	Vascular endothelial cell growth factor**	193.50±21.64	255±9.53	0.76
MCP-5	Monocyte chemoattractant protein-5**	228.7±20.43	352±38.66	0.65
TIMP-1	Tissue inhibitor of metalloproteinase type-1*	15500±2150	1930±570	8.03
LIF	Leukemia inhibitory factor*	45.37±9.68	30.47±2.89	1.49
EGF	Epidermal growth factor**	2.79±0.47	1.59±0.14	1.75
MDC	Macrophage-derived chemokine*	36.4±9.80	21.97±0.99	1.66
MIP-3	Macrophage inflammatory protein-3beta**	82±13	58±5	1.41
TPO	Thrombopoietin*	2150±170	1900±100	1.13

addition, intercellular signaling molecules (cytokines/chemokines) measured in the amniotic fluid, revealed a high inflammatory reaction on day 16 *p.c.*, indicating that even after the irradiation exposure, fetal growth continues in a hostile environment that could lead to secondary apoptosis via intercellular communication.

In the present study, the full abnormal phenotype was recorded at day 19 *p.c.* However, the genesis of the forelimb defects was scored at different time points during development (days 14, 15, 16 and 17 *p.c.*) and the first signs of maldevelopment were observed at days 16 and 17 *p.c.* Normal development of digits is an ordered process of cell division, differentiation and cell death that is programmed both spatially and temporally. Induction of apoptosis in the predigital regions and limb digital defects by prenatal irradiation depend on both p53 gene status and radiation dose. Radiation selectively kills the cells in the predigital regions by p53-dependent apoptosis, and excessive cell death results in failure of limb buds to develop, which finally leads to digital defects (Wang, 2001). Studies with chemicals have also suggested that excessive cell death for which the embryo may be unable to compensate could represent an important mechanism of limb defects (Sulik and Dehart, 1988; Kochhar et al., 1978; Ritter et al., 1973).

Involvement of the stress signaling pathway (MAPK) in radiation-induced forelimb defects

This pathway mediates signal transduction from cell surface to the nucleus as a response to stress stimuli such as cytokines, radiation, heat and osmotic shocks. It is involved in proliferation, senescence, differentiation and apoptosis (Kumar et al., 2004; Davis, 2000; Fanger, 1999; Schaeffer and Weber, 1999; Minden and Karin, 1997, Dent et al., 1999, 2003; Wang et al., 2000; Widmann et al., 1998; Rosette and Karin, 1996).

Distinct members of the protein kinase family called MAPK kinases (MAPKKs) control this stress pathway. Indeed, JNK (C-JUN N-terminal Kinase) is activated by MKK4 and MKK3 through MKK7 phosphorylation, while p38 is directly activated by MKK3 and MKK6 (Deacon and Blank, 1999; Makeeva et al., 2006; Wang et al., 2002; Deacon and Blank, 1999; Blank et al., 1996).

The function of MAPK kinases during development is not well documented. However, it has been shown that mouse mutants for the MKK4 protein are not viable as a consequence of skeletal malformations and defects in the neural tube closure (Abell et al., 2005). Likewise, MKK3 null mice are not viable and die from a disturbed vasculogenesis at day 11 *p.c.* (Yang et al., 2000). In addition, MKK3 was shown to play an important role in many functions among which: cell protection mechanisms and anti-inflammation (Ellinger-Ziegelbauer et al., 1999; Otterbein et al., 2003).

In our study, MKK3 has been found to be overexpressed in the irradiated fetuses with forelimb defects (Fig. 9A). As MKK3 seems to be involved in many important processes besides development, one can imagine a possible association between MKK3 activation and the occurrence of apoptosis and later on forelimb defects in the irradiated fetuses. MKK3 would potentially act via its downstream targets, such as JNK and/or p38. The later can trigger either cell proliferation or cellular death which is likely behind forelimb defects observed later on during development.

As mentioned above, MKK7 is a specific activator of JNK signaling cascade that directs cells toward proliferation, differentiation, transformation or apoptosis. In mice, MKK7 inactivation results in altered hepatocyte proliferation and embryonic lethality. *In vitro*, embryonic fibroblasts bearing inactive MKK7, fail to proliferate, senesce prematurely and show G2/M cell cycle arrest (Wada et al., 2004; Wada and Penninger, 2004). In our study, MKK7 was found to be highly expressed in the fetuses 24 h after irradiation. It is therefore possible that under condition of environmental stress, overexpression of MKK7 maintains the proliferative state of the cells, potentially, through JNK signaling, but this must be checked in future studies.

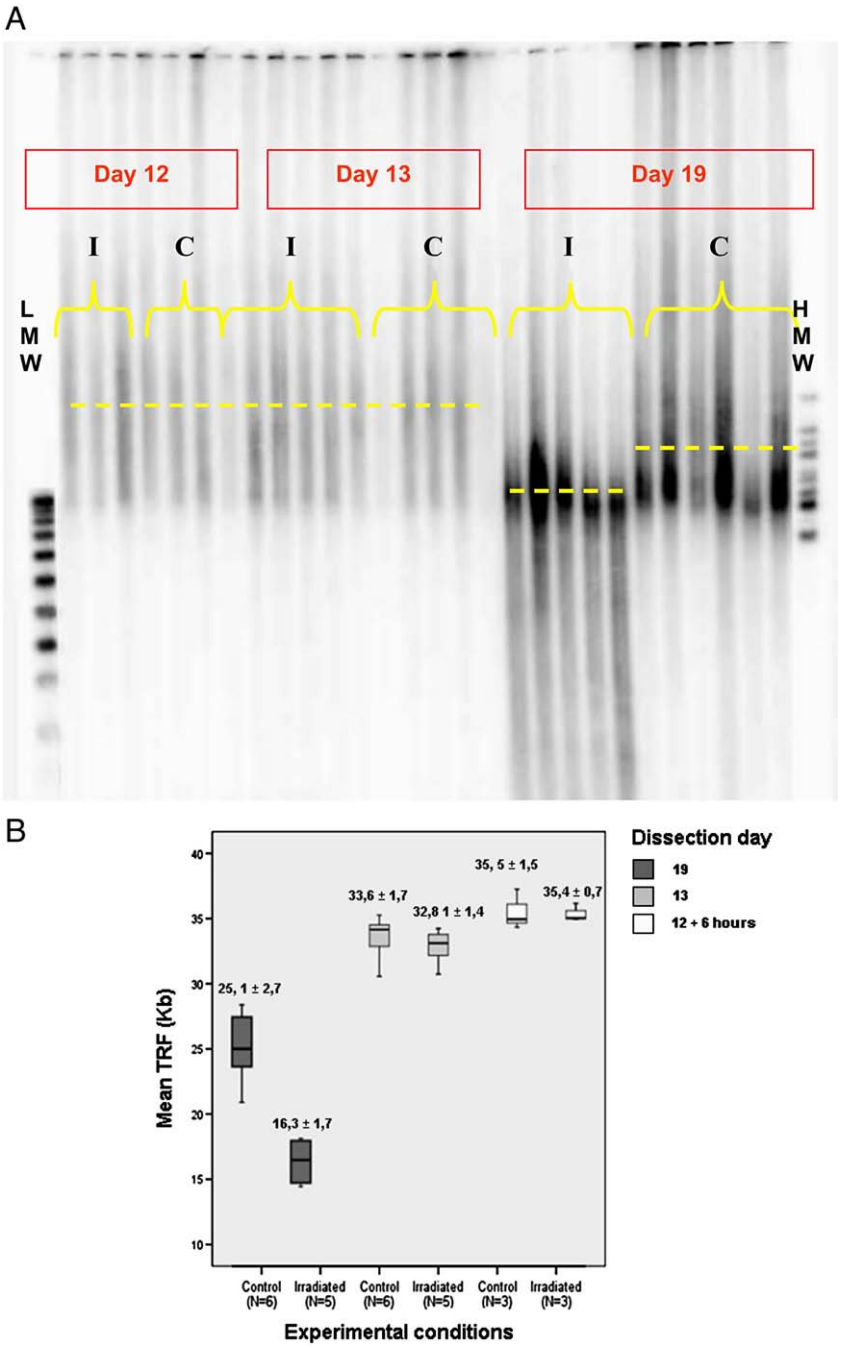

Fig. 8. Telomere lengths in fetuses at days 12, 13 and 19 *p.c.* (A) A southern blot of TRF length analysis of telomeres of control and irradiated fetuses at days 12, 13 and 19 *p.c.* Only at day 19 *p.c.* is a pronounced shortening of telomeres observed in irradiated fetuses vs. controls (I: irradiated; C: control; LMW: low molecular weight; HMW: high molecular weight). Dashed lines correspond to average location of the band. (B) TRF values of control and irradiated fetuses. The numbers on top of each box are the average values ± the standard deviation.

Radiation-induced forelimb defects are associated with an enhanced inflammatory reaction in the amniotic fluid

Cytokine and chemokines are soluble proteins that are involved in every facet of immunity and inflammation. Furthermore, they have been shown to regulate different processes during development such as implantation (Sharkey, 1998) trophoblast invasiveness, tissue remodeling during placental development (Librach et al., 1994) and the onset of labor (Orsi et al., 2007). In our study, the irradiated fetuses suffered from a chronic inflammation mediated by pro-inflammatory cytokines and chemokines. As late as 4 days after irradiation, we could measure the high presence of pro-inflammatory cytokines/chemokines in the amniotic fluid. According to our gene expression data, this inflammatory process must have been initiated much earlier during development. Indeed, overexpression of genes (i.e. MCP-1, IP-10 CD 40 and IL-6) that code for some of the pro-inflammatory proteins found in the amniotic fluid was already measured in the irradiated forelimb tissues as soon as 24 h post-irradiation. This observation, suggests a role for the inflammatory proteins in the early fetal response toward irradiation and potentially in radiation-induced forelimb defects.

Besides MCP-1, IP-10, CD40 and IL-6; MCP-3, RANTES and MIP-1α were also highly present in the amniotic fluid (see Table 3). In humans, these ckemokines are shown to be associated with microbial invasion, radiation-induced pulmonary fibrosis, preterm delivery and

inflammation of the amniotic fluid (Jacobsson et al., 2005, 2003; Johnston et al., 2002; Athayde et al., 1999; Romero et al., 1994). In our model, those chemokines might be considered as markers of inflammation and low weight at birth.

TNF-α and IFN-γ were also highly present in the amniotic fluid of irradiated fetuses. Those two cytokines act synergistically to initiate a chronic inflammation. TNF-α but not IFN-γ was associated with increased fetal death in mice subjected to hyperthermia stress during the organogenesis period (Kumar et al., 2006). In addition, TNF-α is known to mediate apoptosis, of which excess is linked with embryonic malformation and loss (Brill et al., 1999). Therefore, involvement of TNF-α in forelimb defects can not be excluded.

Telomere shortening is associated with forelimb defects

Dysfunctional telomeres are known to be involved in DNA damage response, cell cycle arrest, senescence, apoptosis and chromosome end fusions. Yet little is known about telomere dynamics during intrauterine life and their contribution to particular developmental defects. (Bekaert et al., 2004; Youngren et al., 1998; Prowse and Greider, 1995). In our study, telomere shortening in irradiated/malformed fetuses was observed solely at day 19 *p.c.* as opposed to control fetuses (Figs. 8A and B). Interestingly, telomere shortening was observed as hypodactyly became apparent (Figs. 6 and 8B). We showed previously an association between radiation-induced polymorphous malformations, p53 status and telomere shortening (Bekaert et al., 2005; Baatout et al., 2002). In this new study, our data suggest that forelimb defects and digital losses are featured by telomere shortening.

Several studies have linked telomere shortening to various inflammation-related pathogeneses such as rheumatoid arthritis, inflammatory bowel diseases, and prostate cancer (Risques et al., 2006; Ramirez et al., 2005; De Marzo et al., 2003; O'Sullivan et al., 2002; Kinouchi et al., 1998). Likewise in our study, telomere

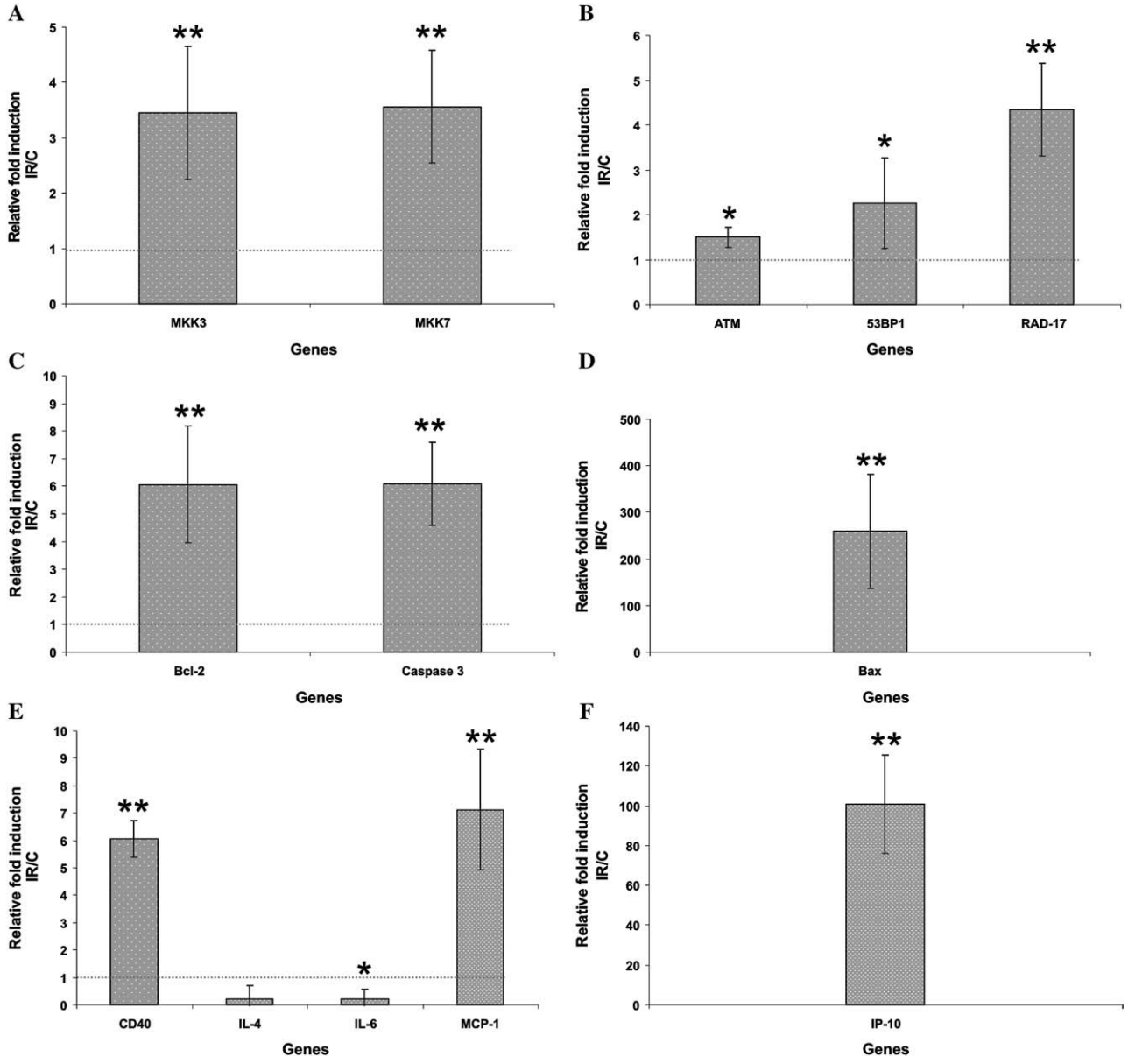

Fig. 9. Relative gene expression measured by RT-q-PCR in irradiated (IR) forelimb bud tissues as compared to controls (C), 24 h following irradiation. The various levels of genes involved in: mitogen activated protein kinase (MAPK) proliferative pathway (MKK3, MKK7) (A), the DNA damage response pathway (ATM, Rad17, 53BP1) (B), the apoptotic pathway (anti-apoptotic Bcl-2 and pro-apoptotic caspase-3 and Bax) (C, D), and pro-inflammatory cytokines and chemokines (CD40, IL-4, IL-6, MCP-1, and IP-10) (E, F). *$p<0.05$; **$p<0.01$).

shortening observed in fetuses at day 19 *p.c.* is associated to an inflammatory reaction as evidenced by the high level of pro-inflammatory cytokines measured in the amniotic fluid.

Taken together, in our study, ATM, Rad17 and 53BP1 were found highly expressed in the irradiated fetuses before telomere shortening becomes detectable. This indicates the presence of a DNA repair mechanism before the cells reach a critical situation, featured by telomere shortening. Interestingly, these DNA repair proteins have been previously associated with telomere maintenance and have been shown to accumulate at uncapped telomeres (Longhese, 2008; Slijepcevic and Al-Wahiby, 2005; Takai et al., 2003). In the future, it would be of interest to co-monitor the timing of telomere shortening and the localization of these DNA repair proteins to know whether the cellular response to uncapped telomere might be governed by the DNA damage proteins in our model of forelimb defects.

Conclusion

In this study, we explored the morphological and molecular changes associated with radiation-induced forelimb defects during late organogenesis.

Our data suggest that following irradiation, DNA repair mechanisms (Rad17, ATM and 53BP1) as well as antagonist mechanisms that prone either cellular proliferation (Bcl-2 and MKK7) or cellular death (Bax, caspase-3 and MKK3) are activated. This might be an explanation for the distinct severity of the observed forelimb defects. In addition, we measured an early and late inflammatory response, which probably sustains via MAPK pathway the hostile environment generated by apoptosis and in which the fetuses continue their development.

While monitoring the fetuses for the development of forelimb defects during development, we noticed that the full abnormal phenotype was concomitant with detectable telomere shortening, indicating a critical cellular situation. We believe in an association between telomere shortening and the timing of the appearance of malformation during development. However, this should be investigated in future studies by exploring telomere length at additional time points during development.

Acknowledgments

The authors are grateful to Prof. Dr. Max Mergeay and Prof. Dr. Patrick van Oostveldt for the fruitful discussion and support. The authors are also indebted to Mr. Eddy Aerts and Mr. Eddy Wuyts for their daily help concerning the animal care. The authors would finally like to thank Mr. Dirk Delnooz and Mr. Swat Janssens for their help in editing the figures depicted in this paper. This work is supported by research contracts from the European Union under the Nuclear Euratom Programme (FIS5-2002-00029 and FI6R-2006-036465).

References

Abell, A.N., Rivera-Perez, J.A., Cuevas, B.D., Uhlik, M.T., Sather, S., Johnson, N.L., Minton, S.K., Lauder, J.M., Winter-Vann, A.M., Nakamura, K., Magnuson, T., Vaillancourt, R.R., Heasley, L.E., Johnson, G.L., 2005. Ablation of MEKK4 kinase activity causes neurulation and skeletal patterning defects in the mouse embryo. Mol. Cell Biol. 25, 8948–8959.

Athayde, N., Romero, R., Maymon, E., Gomez, R., Pacora, P., Araneda, H., Yoon, B.H., 1999. A role for the novel cytokine RANTES in pregnancy and parturition. Am. J. Obstet. Gynecol. 181, 989–994.

Baatout, S., Jacquet, P., Michaux, A., Buset, J., Vankerkom, J., Derradji, H., Yan, J., von Suchodoletz, H., de Saint-Georges, L., Desaintes, C., Mergeay, M., 2002. Developmental abnormalities induced by X-irradiation in p53 deficient mice. In Vivo 16, 215–221.

Bamias, G., Nyce, M.R., De La Rue, S.A., Cominelli, F., 2005. New concepts in the pathophysiology of inflammatory bowel disease. Ann. Intern. Med. 143, 895–904.

Bartha, J.L., Romero-Carmona, R., Comino-Delgado, R., 2003. Inflammatory cytokines in intrauterine growth retardation. Acta. Obstet. Gynecol. Scand. 82, 1099–1102.

Bekaert, S., Derradji, H., Baatout, S., 2004. Telomere biology in mammalian germ cells and during development. Dev. Biol. 274, 15–30.

Bekaert, S., Derradji, H., De Meyer, T., Michaux, A., Buset, J., Neefs, M., Mergeay, M., Jacquet, P., Van Oostveldt, P., Baatout, S., 2005. Telomere shortening is associated with malformation in p53-deficient mice after irradiation during specific stages of development. DNA Repair (Amst). 4, 1028–1037.

Bekaert, S., De Meyer, T., Rietzschel, E.R., De Buyzere, M.L., De Bacquer, D., Langlois, M., Segers, P., Cooman, L., Van Damme, P., Cassiman, P., et al., 2007. Telomere length and cardiovascular risk factors in a middle-aged population free of overt cardiovascular disease. Aging Cell 6, 639–647.

Blank, J.L., Gerwins, P., Elliott, E.M., Sather, S., Johnson, G.L., 1996. Molecular cloning of mitogen-activated protein/ERK kinase kinases (MEKK) 2 and 3. Regulation of sequential phosphorylation pathways involving mitogen-activated protein kinase and c-Jun kinase. J. Biol. Chem. 271, 5361–5368.

Boreham, D.R., Dolling, J.A., Misonoh, J., Mitchel, R.E., 2002. Radiation-induced teratogenic effects in fetal mice with varying Trp53 function: influence of prior heat stress. Radiat. Res. 158, 449–457.

Brill, A., Torchinsky, A., Carp, H., Toder, V., 1999. The role of apoptosis in normal and abnormal embryonic development. J. Assist. Reprod. Genet. 16, 512–519.

Davis, R.J., 2000. Signal transduction by the JNK group of MAP kinases. Cell 103, 239–252.

De Marzo, A.M., Meeker, A.K., Zha, S., Luo, J., Nakayama, M., Platz, E.A., Isaacs, W.B., Nelson, W.G., 2003. Human prostate cancer precursors and pathobiology. Urology 62, 55–62.

Deacon, K., Blank, J.L., 1999. MEK kinase 3 directly activates MKK6 and MKK7, specific activators of the p38 and c-Jun NH2-terminal kinases. J. Biol. Chem. 274, 16604–16610.

Dent, P., Reardon, D.B., Park, J.S., Bowers, G., Logsdon, C., Valerie, K., Schmidt-Ullrich, R., 1999. Radiation-induced release of transforming growth factor alpha activates the epidermal growth factor receptor and mitogen-activated protein kinase pathway in carcinoma cells, leading to increased proliferation and protection from radiation-induced cell death. Mol. Biol. Cell 10, 2493–2506.

Dent, P., Yacoub, A., Fisher, P.B., Hagan, M.P., Grant, S., 2003. MAPK pathways in radiation responses. Oncogene 22, 5885–5896.

Dlugosz, P.J., Billen, L.P., Annis, M.G., Zhu, W., Zhang, Z., Lin, J., Leber, B., Andrews, D.W., 2006. Bcl-2 changes conformation to inhibit Bax oligomerization. Embo J. 25, 2287–2296.

Ellinger-Ziegelbauer, H., Kelly, K., Siebenlist, U., 1999. Cell cycle arrest and reversion of Ras-induced transformation by a conditionally activated form of mitogen-activated protein kinase kinase kinase 3. Mol. Cell Biol. 19, 3857–3868.

Esplin, M.S., Romero, R., Chaiworapongsa, T., Kim, Y.M., Edwin, S., Gomez, R., Mazor, M., Adashi, E.Y., 2005. Monocyte chemotactic protein-1 is increased in the amniotic fluid of women who deliver preterm in the presence or absence of intra-amniotic infection. J. Matern. Fetal Neonatal Med. 17, 365–373.

Fanger, G.R., 1999. Regulation of the MAPK family members: role of subcellular localization and architectural organization. Histol. Histopathol. 14, 887–894.

Farber, J.L., Kyle, M.E., Coleman, J.B., 1990. Mechanisms of cell injury by activated oxygen species. Lab. Invest. 62, 670–679.

Gavrieli, Y., Sherman, Y., Ben-Sasson, S.A., 1992. Identification of programmed cell death in situ via specific labeling of nuclear DNA fragmentation. J. Cell Biol. 119, 493–501.

Goepfert, A.R., Andrews, W.W., Carlo, W., Ramsey, P.S., Cliver, S.P., Goldenberg, R.L., Hauth, J.C., 2004. Umbilical cord plasma interleukin-6 concentrations in preterm infants and risk of neonatal morbidity. Am. J. Obstet. Gynecol. 191, 1375–1381.

Jacobsson, B., Holst, R.M., Wennerholm, U.B., Andersson, B., Lilja, H., Hagberg, H., 2003. Monocyte chemotactic protein-1 in cervical and amniotic fluid: relationship to microbial invasion of the amniotic cavity, intra-amniotic inflammation, and preterm delivery. Am. J. Obstet. Gynecol. 189, 1161–1167.

Jacobsson, B., Holst, R.M., Andersson, B., Hagberg, H., 2005. Monocyte chemotactic protein-2 and -3 in amniotic fluid: relationship to microbial invasion of the amniotic cavity, intra-amniotic inflammation and preterm delivery. Acta. Obstet. Gynecol. Scand. 84, 566–571.

Jacquet, P., de Saint-Georges, L., Vankerkom, J., Baugnet-Mahieu, L., 1995. Embryonic death, dwarfism and fetal malformations after irradiation of embryos at the zygote stage: studies on two mouse strains. Mutat. Res. 332, 73–87.

Johnston, C.J., Williams, J.P., Okunieff, P., Finkelstein, J.N., 2002. Radiation-induced pulmonary fibrosis: examination of chemokine and chemokine receptor families. Radiat. Res. 157, 256–265.

Kimmel, C.A., Trammell, C., 1981. A rapid procedure for routine double staining of cartilage and bone in fetal and adult animals. Stain Technol. 56, 271–273.

Kinouchi, Y., Hiwatashi, N., Chida, M., Nagashima, F., Takagi, S., Maekawa, H., Toyota, T., 1998. Telomere shortening in the colonic mucosa of patients with ulcerative colitis. J. Gastroenterol. 33, 343–348.

Kochhar, D.M., Penner, J.D., McDay, J.A., 1978. Limb development in mouse embryos. II. Reduction defects, cytotoxicity and inhibition of DNA synthesis produced by cytosine arabinoside. Teratology 18, 71–92.

Kumar, P., Miller, A.I., Polverini, P.J., 2004. p38 MAPK mediates gamma-irradiation-induced endothelial cell apoptosis, and vascular endothelial growth factor protects endothelial cells through the phosphoinositide 3-kinase-Akt-Bcl-2 pathway. J. Biol. Chem. 279, 43352–43360.

Kumar, P., Rathore, B., Saxena, A.K., Purohit, D.C., Mathur, N., Paul, B.N., 2006. Role of TNF-alpha in prenatal alterations in dams of mice under thermal stress. Lab. Anim. 40, 172–179.

Kurishita, A., 1989. Histological study of cell death in digital malformations induced by 5-azacytidine: suppressive effect of caffeine. Teratology 39, 163–172.

Layton Jr., W.M., Hallesy, D.W., 1965. Forelimb deformity in rats: association with acetazolamide. Science 150, 79.

Librach, C.L., Feigenbaum, S.L., Bass, K.E., Cui, T.Y., Verastas, N., Sadovsky, Y., Quigley, J.P.,

French, D.L., Fisher, S.J., 1994. Interleukin-1 beta regulates human cytotrophoblast metalloproteinase activity and invasion in vitro. J. Biol. Chem. 269, 17125–17131.
Longhese, M.P., 2008. DNA damage response at functional and dysfunctional telomeres. Genes Dev. 22, 125–140.
Makeeva, N., Myers, J.W., Welsh, N., 2006. Role of MKK3 and p38 MAPK in cytokine-induced death of insulin-producing cells. Biochem. J. 393, 129–139.
Minden, A., Karin, M., 1997. Regulation and function of the JNK subgroup of MAP kinases. Biochim. Biophys. Acta 1333, F85–104.
Norimura, T., Nomoto, S., Katsuki, M., Gondo, Y., Kondo, S., 1996. p53-dependent apoptosis suppresses radiation-induced teratogenesis. Nat. Med. 2, 577–580.
Oboh, A.E., Orsi, N.M., Campbell, J., 2006. Amniotic fluid cytokine profile in association with fetal hyperechogenic bowel. Eur. J. Obstet. Gynecol. Reprod. Biol. 128, 86–90.
Orsi, N.M., Gopichandran, N., Ekbote, U.V., Walker, J.J., 2006. Murine serum cytokines throughout the estrous cycle, pregnancy and post partum period. Anim. Reprod. Sci. 96, 54–65.
Orsi, N.M., Gopichandran, N., Bulsara, H., Ekbote, U.V., Walker, J.J., 2007. Regulation of maternal serum and amniotic fluid cytokine profiles in the mouse: possible roles in the onset of labour. J. Reprod. Immunol. 75, 97–105.
O'Sullivan, J.N., Bronner, M.P., Brentnall, T.A., Finley, J.C., Shen, W.T., Emerson, S., Emond, M.J., Gollahon, K.A., Moskovitz, A.H., Crispin, D.A., Potter, J.D., Rabinovitch, P.S., 2002. Chromosomal instability in ulcerative colitis is related to telomere shortening. Nat. Genet. 32, 280–284.
Otterbein, L.E., Otterbein, S.L., Ifedigbo, E., Liu, F., Morse, D.E., Fearns, C., Ulevitch, R.J., Knickelbein, R., Flavell, R.A., Choi, A.M., 2003. MKK3 mitogen-activated protein kinase pathway mediates carbon monoxide-induced protection against oxidant-induced lung injury. Am. J. Pathol. 163, 2555–2563.
Pampfer, S., Streffer, C., 1989. Increased chromosome aberration levels in cells from mouse fetuses after zygote X-irradiation. Int. J. Radiat. Biol. 55, 85–92.
Porter, A.E., Auth, J., Prince, M., Ghidini, A., Brenneman, D.E., Spong, C.Y., 2001. Optimization of cytokine stability in stored amniotic fluid. Am. J. Obstet. Gynecol. 185, 459–462.
Prowse, K.R., Greider, C.W., 1995. Developmental and tissue-specific regulation of mouse telomerase and telomere length. Proc. Natl. Acad. Sci. U. S. A. 92, 4818–4822.
Ramirez, R., Carracedo, J., Soriano, S., Jimenez, R., Martin-Malo, A., Rodriguez, M., Blasco, M., Aljama, P., 2005. Stress-induced premature senescence in mononuclear cells from patients on long-term hemodialysis. Am. J. Kidney Dis. 45, 353–359.
Renfree, M.B., Hensleigh, H.C., McLaren, A., 1975. Developmental changes in the composition and amount of mouse fetal fluids. J. Embryol. Exp. Morphol. 33, 435–446.
Risques, R.A., Rabinovitch, P.S., Brentnall, T.A., 2006. Cancer surveillance in inflammatory bowel disease: new molecular approaches. Curr. Opin. Gastroenterol. 22, 382–390.
Ritter, E.J., Scott, W.J., Wilson, J.G., 1973. Relationship of temporal patterns of cell death and development to malformations in the rat limb. Possible mechanisms of teratogenesis with inhibitors of DNA synthesis. Teratology 7, 219–225.
Romero, R., Gomez, R., Galasso, M., Munoz, H., Acosta, L., Yoon, B.H., Svinarich, D., Cotton, D.B., 1994. Macrophage inflammatory protein-1 alpha in term and preterm parturition: effect of microbial invasion of the amniotic cavity. Am. J. Reprod. Immunol. 32, 108–113.
Rosette, C., Karin, M., 1996. Ultraviolet light and osmotic stress: activation of the JNK cascade through multiple growth factor and cytokine receptors. Science 274, 1194–1197.
Sarkar, D., Fisher, P.B., 2006. Molecular mechanisms of aging-associated inflammation. Cancer Lett. 236, 13–23.
Schaeffer, H.J., Weber, M.J., 1999. Mitogen-activated protein kinases: specific messages from ubiquitous messengers. Mol. Cell Biol. 19, 2435–2444.
Sharkey, A., 1998. Cytokines and implantation. Rev. Reprod. 3, 52–61.
Slijepcevic, P., Al-Wahiby, S., 2005. Telomere biology: integrating chromosomal end protection with DNA damage response. Chromosoma 114, 275–285.
Streffer, C., 2006. Transgenerational transmission of radiation damage: genomic instability and congenital malformation. J. Radiat. Res. (Tokyo) 47 (Suppl B), B19–24.
Sulik, K.K., Dehart, D.B., 1988. Retinoic-acid-induced limb malformations resulting from apical ectodermal ridge cell death. Teratology 37, 527–537.
Takai, H., Smogorzewska, A., de Lange, T., 2003. DNA damage foci at dysfunctional telomeres. Curr. Biol. 13, 1549–1556.
Tiboni, G.M., Iammarrone, E., Piccirillo, G., Liberati, M., Bellati, U., 1998. Aspirin pretreatment potentiates hyperthermia-induced teratogenesis in the mouse. Am. J. Obstet. Gynecol. 178, 270–279.
Wada, T., Penninger, J.M., 2004. Stress kinase MKK7: savior of cell cycle arrest and cellular senescence. Cell Cycle 3, 577–579.
Wada, T., Joza, N., Cheng, H.Y., Sasaki, T., Kozieradzki, I., Bachmaier, K., Katada, T., Schreiber, M., Wagner, E.F., Nishina, H., Penninger, J.M., 2004. MKK7 couples stress signalling to G2/M cell-cycle progression and cellular senescence. Nat. Cell Biol. 6, 215–226.
Wang, B., 2001. Involvement of p53-dependent apoptosis in radiation teratogenesis and in the radioadaptive response in the late organogenesis of mice. J. Radiat. Res. (Tokyo) 42, 1–10.
Wang, B., Fujita, K., Ohhira, C., Watanabe, K., Odaka, T., Mitani, H., Hayata, I., Ohyama, H., Yamada, T., Shima, A., 1999. Radiation-induced apoptosis and limb teratogenesis in embryonic mice. Radiat. Res. 151, 63–68.
Wang, B., Ohyama, H., Haginoya, K., Odaka, T., Yamada, T., Hayata, I., 2000. Prenatal radiation-induced limb defects mediated by Trp53-dependent apoptosis in mice. Radiat. Res. 154, 673–679.
Wang, L., Ma, R., Flavell, R.A., Choi, M.E., 2002. Requirement of mitogen-activated protein kinase kinase 3 (MKK3) for activation of p38alpha and p38delta MAPK isoforms by TGF-beta 1 in murine mesangial cells. J. Biol. Chem. 277, 47257–47262.
Weissenborn, U., Streffer, C., 1988. Analysis of structural and numerical chromosomal anomalies at the first, second, and third mitosis after irradiation of one-cell mouse embryos with X-rays or neutrons. Int. J. Radiat. Biol. 54, 381–394.
Widmann, C., Gerwins, P., Johnson, N.L., Jarpe, M.B., Johnson, G.L., 1998. MEK kinase 1, a substrate for DEVD-directed caspases, is involved in genotoxin-induced apoptosis. Mol. Cell Biol. 18, 2416–2429.
Yang, J., Boerm, M., McCarty, M., Bucana, C., Fidler, I.J., Zhuang, Y., Su, B., 2000. Mekk3 is essential for early embryonic cardiovascular development. Nat. Genet. 24, 309–313.
Youngren, K., Jeanclos, E., Aviv, H., Kimura, M., Stock, J., Hanna, M., Skurnick, J., Bardeguez, A., Aviv, A., 1998. Synchrony in telomere length of the human fetus. Hum. Genet. 102, 640–643.
Zhou, L., Yuan, R., Serggio, L., 2003. Molecular mechanisms of irradiation-induced apoptosis. Front Biosci. 8, d9–19.